Electrical Power and Energy Systems 133 (2021) 107248

Contents lists available at ScienceDirect

International Journal of Electrical Power and Energy Systems

journal homepage: www.elsevier.com/locate/ijepes

A new monitoring technique for fault detection and classification in PV systems based on rate of change of voltage-current trajectory

Hossam A. Abd el-Ghany [a,*], Ahmed E. ELGebaly [a], Ibrahim B.M. Taha [a,b]

[a] Electrical Power and Machines Engineering Department, Faculty of Engineering, Tanta University, 31521 Tanta, Egypt
[b] Electrical Engineering Department, College of Engineering, Taif University, Taif, 21944, Saudi Arabia

ARTICLE INFO

Keywords:
PV solar system
Rate of change of PV states
Abnormal PV states
MATLAB/Simulink toolbox
PV degradation rate

ABSTRACT

This paper proposes a new simple technique to detect and discriminate the abnormal states of the grid-connected photovoltaic (PV) solar system based on the rate of change of voltage and current trajectory. The design of the PV system is developed by implementation of only one diode in every PV string. The diode prevents the reverse direction of the fault current in case of faulty strings. On the other hand, the installation of a diode reduces the ability of faults detection and diagnosis depending on currents in each string. The proposed technique depends on the rate of change of voltages and current trajectory during the fault transient period. The proposed algorithm can detect various fault cases such as cell-to-cell and string to string faults in addition to partial and full shadow faults. Also, the algorithm differentiates between high and low fault cases for each fault types. Moreover, the proposed technique is characterized by high sensitivity for internal abnormal states within certain array with high security level for the external abnormal conditions and normal load changing. The proposed technique is applied for a four-array PV system, which has a power rating of 400 kW connected to an AC grid. The simulation results and validation of the proposed technique are implemented by MATLAB/Simulink toolbox. The proposed technique is experimentally applied for a small PV system of a rating of 1.25 kW to prove its validity.

1. Introduction

Photovoltaic (PV) power resources are free-pollution resources of electrical power energy because they do not generate any exhausted contamination [1]. The power generated from the PV systems reached about 300 GW at 2016 (around, 2% of all-over the world generated power), which reached about 627 GW at 2019 (around, 3% of all-over the world generated power) [2–4]. The high initial cost and low efficiency of the PV systems are their two main drawbacks [5]. However, the initial costs are decreased todays compared to the first PV system and the PV system efficiency is enhanced to reach up to 40%, especially when connected to AC grid systems [5].

Connections between PV system and AC-grids are carried out by inverters. The PV system modules are directly aligned to the sun directions to obtain maximum power. The orientation of PV system modules to the sun's direction is carried out by solar trackers, which adjust the PV system to be vertical with sun's lights during daytime. Also, the maximum power tracking approach is used for extracting maximum power from the PV modules [6–8]. Furthermore, grid-connected PV systems are used to reduce both distribution and transmission losses.

Monitoring the PV systems today is very essential due to their rapid expansion for different purposes and applications. Monitoring the PV system is used to detect their faults, which affect operating states and performance [9].

Some published works suggested different algorithms to monitor and detect the PV system faults [10–27]. In [10–16], fault detection algorithms are built based on PV system parameters. The electrical data and temperature for the algorithm presented in [10] are collected by energy balance equation to determine the PV system fault based on PV system parameters. The model in [11] is built based on the signal of irradiation and temperature sensors to reduce the signal required for fault detection model, while the effect of partial shadow on the array voltage and current with the power losses is used as an indicator to determine the PV system fault types as expressed in [12]. In [13], a fault detection model is built based on the evaluation of parameters that characterize the V-I curve of the PV system. The model developed in [14] is built based on measured irradiation and the PV array temperature model are used to check the measured data to enhance the presented fault detection model. In [15], the ratio between measured and theoretically-calculated

* Corresponding author.
E-mail addresses: hossam.saleh@f-eng.tanta.edu.eg (H.A. Abd el-Ghany), ahmed.elgebaly@f-eng.tanta.edu.eg (A.E. ELGebaly), i.taha@tu.edu.sa (I.B.M. Taha).

https://doi.org/10.1016/j.ijepes.2021.107248
Received 4 January 2021; Received in revised form 22 March 2021; Accepted 8 May 2021
Available online 4 June 2021

PV system output power and the voltage ratios are used as indicators of fault types in grid-connected PV systems, while in [16], the digital twin concept is used to build the PV system fault model. The twin model is a physical model that is used to estimate, in real time, the PV system characteristics.

Some researches built their detecting fault algorithms depending on the artificial neural systems, fuzzy logic and neuro-fuzzy approaches [17–20]. In [17], a Neuro-fuzzy model is built based on six I-V characteristic PV module curves. The status of the PV system is determined based on the comparisons between the norms parameter values and the threshold values. The model presented in [18] is built based on a probabilistic neural network. The model is trained by the predicted and classified faults normalized datasets with high predicting accuracy. In [19], the fault model for predicting the PV system fault is based on a convolution neural network (CNN). The CNN model is built based on four-layer structure module. It identifies the different PV fault types with high detecting accuracy. In [20], the presented model is built based on two classification approaches (neural pattern recognition and bagged tree ensemble methods) and utilizing two diodes at the two ends of each string. The two proposed models have high predicting fault accuracy, especially the neural pattern recognition networks.

Different published researches predicted the PV system faults based on machine learning algorithms [21–26]. In [21], the detecting model is constructed based on the kernel based extreme learning machine (KELM). The different detected faults are open circuit faults, short circuit faults, partial shading conditions and degradation faults with high detecting accuracy. The presented model in [22] is built based on wavelet combined with support vector machine. The model has a fast-time predicting accuracy with different PV system faults. In [23], a machine learning model based on Gaussian process regression (GPR) is built to detect the PV system faults. It fastly detects various faults for different PV systems. The model in [24] represents a reduced Kernel Random Forest technique for fault prediction and classification of grid-connected PV system. It has two stages; the first is a feature reduction, while the second stage is a fault classification. It has a high fault predicting accuracy with fast detecting time. In [25], a PV system fault detecting model is built based on a stacked autoencoder (SAE) model. The presented model has a very high detecting accuracy for single failure and multiple failure faults compared to other machine learning approaches. A hybrid artificial bee colony with semi-supervised extreme learning machine algorithm is presented in [26]. The model uses a small amount of data, which reduces costs and detecting time.

The main drawback of most recently published works regarding grid-connected PV systems for fault detections is the dependency on artificial intelligence or machine learning methods, which requires large-case studies and time for training and testing the suggested models. Therefore, a simple detecting approach for grid-connected PV faults is very important to facilitate the detecting process without the requirements of complicated processes or classification methods.

In [20], an approach is constructed by inserting two diodes in each PV string. The prevention of high array currents during faults is the main target of diodes' installation. For each string, only one diode at the upper terminal is enough to accomplish this target. The only function of the down diode is the differentiation between the cell–cell and cell-negative terminal faults. In addition, the detection of the string faults is achieved by using two artificial intelligence (AI) approaches in additional to neural pattern recognition techniques with bagged ensemble trees. These techniques are complicated and need large training samples for good training performance, while (276 cases) are used for training process, which is not enough for adequate training.

Some researchers introduced PV fault diagnosis based on waveform shapes [27–29]. In [27], a voltage-based protection algorithm is presented to classify different string faults and shadow faults. It depended on measuring the voltage across upper and lower cells of each string besides measuring the inverter terminal voltage in the PV array side. The model suggested some conditions of each fault type. The model successfully detects different PV fault types and shadow faults but there are some drawbacks of this model. The model requires several constraints to differentiate between the partial shadow and array faults that represents a model complexity. Consequently, additional constraints are needed to classify the different array fault types. The suggested model in [28] is built based on the normalized super-imposed component of the array power to predict the internal faults of the PV array and the partial shadow. Two steps are required for the fault detection process. In the first step, the fault disturbance is detected while, in the second step, the classification of a fault condition and partial shadow is distinguished. The main shortages in this work are the complexity of the suggested model, there are no distinctions between different internal faults of the PV system and the small size of the used PV system. In [29], a sensorless predicting model is suggested depending on the current decrease between the two sampling instances of maximum power point tracking (MPPT). The suggested model has less fault detecting time with high accuracy. The main shortages of this work are the complexity of the suggested model and neglecting the distinction between low and high cell-to-cell and string-to-string fault types. In addition, string-to-the ground (pole to pole) faults are not implemented.

This paper introduces a new simple protection technique for grid-connected PV system using the rate of changes of voltage ($\Delta V/\Delta t$) and current ($\Delta i/\Delta t$) and mapping them in special phase plan (trajectory). The proposed technique detects all abnormal states and faults in each PV string assisted with only one diode. The proposed approach essential contribution is the installation of only one diode for each PV string installed in the upper terminal of each PV string and monitoring the grid connected PV system without any complicated processes or machine learning approaches. This diode is installed to avoid the inverse of string current direction throughout the fault periods and enable the recognition of faults depending only on the string current and voltage of each string as well as the overall array current and voltage. Based on the diode effect on the faulted PV array, the developed technique determines the types of string faults, such as: cell-to-cell, string-to-string, positive–negative terminal faults as well as the partial and total array shadow as abnormal states. The PV system and the proposed fault detection technique are implemented by MATLAB/Simulink package. The proposed fault detection technique is tested experimentally on various types of abnormal conditions to emphasize its effectiveness to detect and classify them.

2. System description and modeling

The proposed model is developed to simulate a 400 kW grid-connected PV system [20,30], which contains four arrays connected to a 25-kV AC grid via DC/AC inverter and transformer of 0.260/25 kV. Fig. 1 illustrates the construction block diagram of the studied grid-

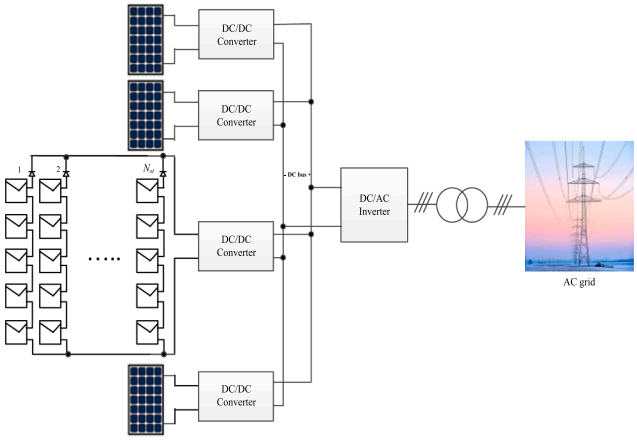

Fig. 1. Block diagram of the PV system assisted with one diode per each string.

connected PV system. Each array is connected to the main DC bus through a DC/DC converter of boost type. The proposed technique is applied on array number three from the top which is expanded as in Fig. 1. The array consists of 68 parallel strings, while each string is assisted by one diode in the upper side. Each string consists of five series-connected PV-cell of type SunPower SPR-315E. For analysis purposes, each cell has a certain number from one to five and the counting started from bottom cell to the top cell. The study measurements are extracted from the first three strings of the array expanded in Fig. 1 The arrays operate according to maximum power point tracking technique (perturb and observe) under any operating condition [30].

This study investigates the system performance under different operation states including steady-state, changing irradiation case, shadow case and different faults regarding cell-to-cell faults, string-to-string faults and positive to negative terminal faults with different values of fault resistance.

The proposed technique depends on the measurement of the current and voltage of each string in additional to array current and voltage. It should be noticed that the string voltage is measured across the PV module excluding the diode. For generalization, the string and array currents and voltages are normalized as in the following equations:

$$i_j = \frac{I_j * N_{st}}{I_t} \tag{1}$$

$$i_{array} = \frac{I_{array}}{I_t} \tag{2}$$

$$V_j = \frac{V_{(m)j}}{V_{st}} \tag{3}$$

$$V_{array} = \frac{V_{(m)array}}{V_{st}} \tag{4}$$

where i_j is the string number j normalized current of measured current I_j, I_t is rated array current, N_{st} is the total number of array strings, which equals 68 for the studied system, i_{array} is the normalized total current of the array, I_{array} is the measured total current of the array, V_j is the normalized string voltage of the measured voltage $V_{(m)j}$, V_{st} is the rated string voltage and v_{array} is the normalized overall array voltage of the measured array voltage $V_{(m)array}$. In this research, the rate of change of normalized currents and voltages represent the key factor to investigate the system abnormal state. The rate of change of each quantity is calculated by dividing the difference between two sampled quantities at sample number k and $k + 1$ by the time interval between these samples Δt. Therefore, the rate of changes of the normalized quantities calculated in (5)–(8) can be given as follows:

$$\frac{\Delta i_j}{\Delta t} = \frac{i_j^{k+1} - i_j^k}{\Delta t} \tag{5}$$

$$\frac{\Delta i_{array}}{\Delta t} = \frac{i_{array}^{k+1} - i_{array}^k}{\Delta t} \tag{6}$$

$$\frac{\Delta V_j}{\Delta t} = \frac{V_j^{k+1} - V_j^k}{\Delta t} \tag{7}$$

$$\frac{\Delta V_{array}}{\Delta t} = \frac{V_{array}^{k+1} - V_{array}^k}{\Delta t} \tag{8}$$

where the superscript (k and $k + 1$) of each quantity means the two successive sample number.

The installation of the diode in the system results in different system performance conditions according to the diode state. The diode may operate in ON or OFF state according to the voltage difference across its terminals. In normal state of operation, the diode works in ON state, while the values of V_j and V_{array} are approximately identical. In some abnormal cases, the diode is in ON state. These cases are characterised by moderate values of voltage rate of change. In this study, these abnormal states are called "low current states" with abbreviation "low + (the abnormal case name)". On the other hand, the abnormal states turn the diodes into OFF state that are called "high current states" with abbreviation "high + (the abnormal case name)". These "high" states are characterised by extreme values of voltage rate of change.

According to Table 1, the states are designated as 0, 1, 2, 3, 4, 5, 6, 7 and 8 for healthy system, high and low cell-to-cell faults, high and low string-to-string faults, high and low shadow states and high and low pole-pole fault, respectively. Generally, the term "high" is used for low fault resistances, whereas "low" is considered for the high fault resistances in case of fault states. For shadow, "low" indicates small shaded area of the array, while "high" means wide shaded area. Fig. 2 illustrates the different abnormal states in accordance with Table 1. It should be noticed that cell-to-cell and string-to-string faults may happen with different combinations not only such as in Fig. 2. The figure illustrates only one cell-to-cell connection between cell number 2 and cell number 4 and illustrates only one string-to-string connection between the second cell in the second string and third cell in the third string. All possible faults connections are conducted in this study. The following section deals with the investigation of the studied system under different operating conditions to conclude the system tendency under different abnormal states.

3. Investigation of system performance under abnormal conditions

The developed detection techniques are modelled using MATLAB/Simulink toolbox [31] for the PV system to determine the system status, which is one of the abnormal states mentioned in Table 1. The performance accuracy of the proposed protection algorithm is determined for various conducted operating statuses. The diagnosis and investigation of various abnormal conditions are carried out by the detection of the voltage and current variations in each string and in the overall array. The trajectory of voltage and current change enables to distinguish between various abnormal states as in the following study.

3.1. Cell to cell fault

Fig. 3 shows the voltage and current of the first and second strings and of the overall array when High cell-to-cell fault with 0 Ω fault resistance is applied between the first and third cells of the first string. A cell-to-cell solidly fault is applied between cells 1 and 3 of the faulted (first) string at 0.2 s. The rate of change of voltage and current for the first and second strings and overall current of array for this state are shown in Fig. 4. As shown in these figures, the voltage of the faulted string is sharply changed from 1p.u. to near zero and, then, slightly increased to settle down around 0.5p.u. On the other hand, the voltages across the healthy string (string 2) and the array (positive to negative terminals) as well as the remining strings are slightly decreased. This is due to the excited diode in the upper terminal of each string, which causes an isolation to the faulted string. This solidly fault causes the anode voltage to be less than the cathode voltage (the diode is in OFF

Table 1
Healthy and abnormal conditions states.

States	Status
0	Healthy system
1	High cell-to-cell fault
2	Low cell-to-cell fault
3	High string-to-string fault
4	Low string-to-string fault
5	High shadow
6	Low shadow
7	High pole-pole fault
8	Low pole-pole fault

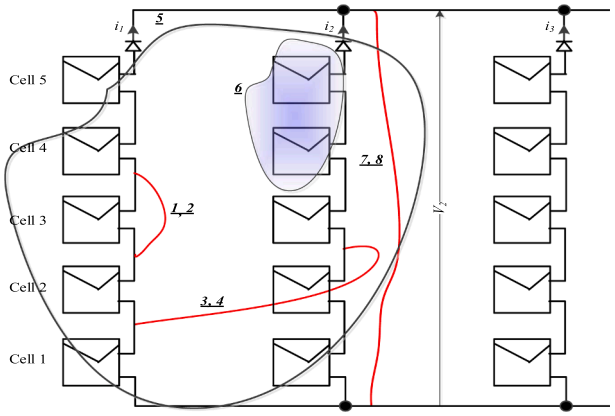

Fig. 2. States of abnormal conditions as in Table 1.

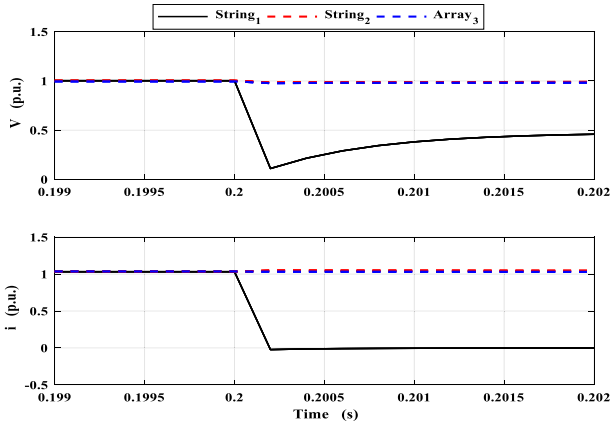

Fig. 3. Voltage and current of the first and second strings and their overall array for first string (High cell-to-cell fault) with 0 Ω between the first cell and the third cell.

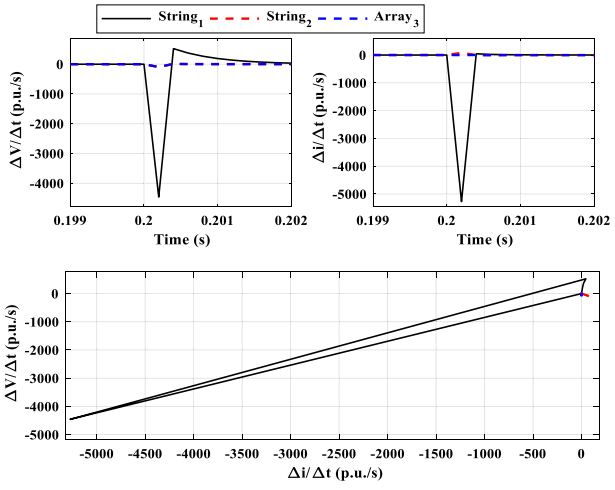

Fig. 4. Rate of change of voltage and current of the first and second strings and overall array for first string (High cell-to-cell fault) with 0 Ω between the first cell and the third cell.

state). This is achieved because the faulted string current is sharply changed from 1p.u. to zero, while the heathy string and array currents are slightly changed around 1p.u. In Fig. 4, the rate of change of voltage and current can be observed due to the suddenly change occurred. The lower part of Fig. 4 represents the relation between the rate of changes of voltage and current. It is concluded that the rate of change of voltage and current are very high for the faulted string, while the healthy strings and overall array are slightly changed around the zero. The maximum values of voltage rate of change for faulty string, healthy string and overall array are −4459.4, −94.9 and −94.9p.u./s, respectively. The maximum values of the rate of change of current for faulty string, healthy string and overall array are −5273.8, 79.24 and −3.7p.u./s, respectively. These values are occurred simultaneously after 0.2 ms from the fault instant. This requires a very fast detection technique.

Figs. 5 and 6 illustrate the voltage and current and their rate of change of the first and second strings and of the overall array when Low cell-to-cell fault with 50 Ω is applied between the first cell and the second cell of the first string. As shown in these figures, contrary to the previous state, the voltage of the faulted string is changed slightly around 1p.u. Also, in the current state, the healthy string (string 2) and the voltage across the array as well as the remining strings are slightly decreased. From these figures, all strings voltages and their rates of change are approximately equal to the faulted one. This reason of this tendency is that the excited diode in the upper terminal of the faulted string will remain in the ON state. As mentioned in this state, the fault occurs with high resistance (50 Ω), which doesn't affect the anode voltage. The maximum values of voltage rate of change of the faulty string, healthy string and overall array are the same and equal to −7.79p.u./s as shown in the lower part of Fig. 6. Consequently, the faulted string current is sharply changed from 1p.u. to around 0.94p.u., while the heathy string and array currents are slightly changed around 1p.u. In this state, the rate of change of the overall array current is positive contrary to the previous state which is negative. The maximum values of current rate of change of faulty string, healthy string and overall array are −469.05, 7.62 and 0.321p.u./s, respectively. It is concluded that the rate of change of current is very high for the faulted string, but the change of voltage is small, while the healthy strings and overall array are slightly changed around the zero.

3.2. String to string fault

Figs. 7 and 8 demonstrate the voltage and current and their rate of change of the first and second strings and overall array. The fault is considered as high string-to-string fault linking between the first cell of the first string and the third cell of the second string with 0 Ω. Here in this state, as shown in these figures, the voltages of the faulted strings are decreased but with different values. The string which has the lowest number of faulted cells from the negative terminal has a lowest value of the voltage related to the other string. However, the healthy strings and the array voltages are slightly decreased. The maximum values of

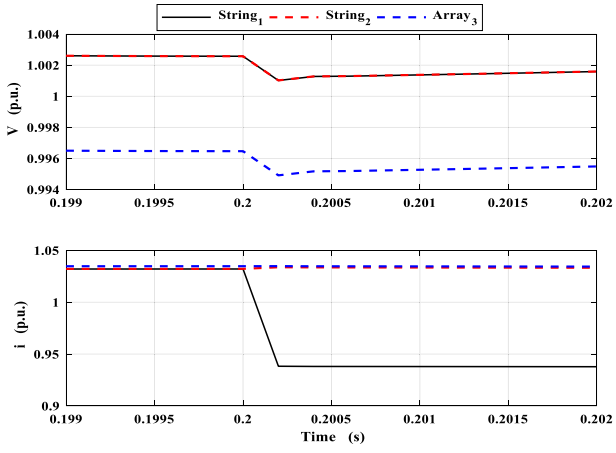

Fig. 5. Voltage and current of the first and second strings and overall array for (Low cell-to-cell) fault with 50 Ω between the first cell and the second cell of the first string.

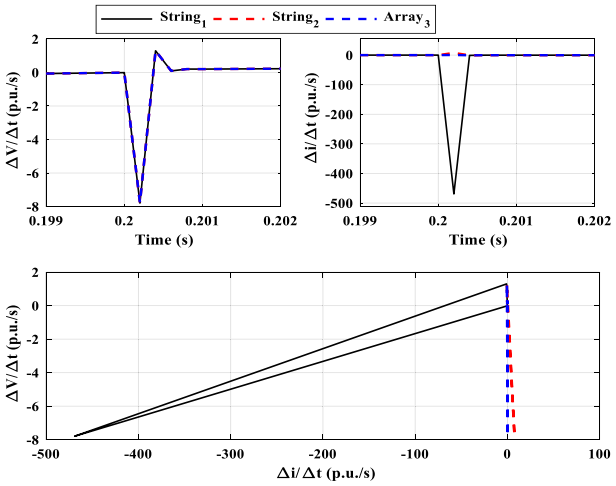

Fig. 6. Rate of change of voltage and current of the first and second strings and overall array for (Low cell-to-cell) fault with 50 Ω between the first cell and the second cell of the first string.

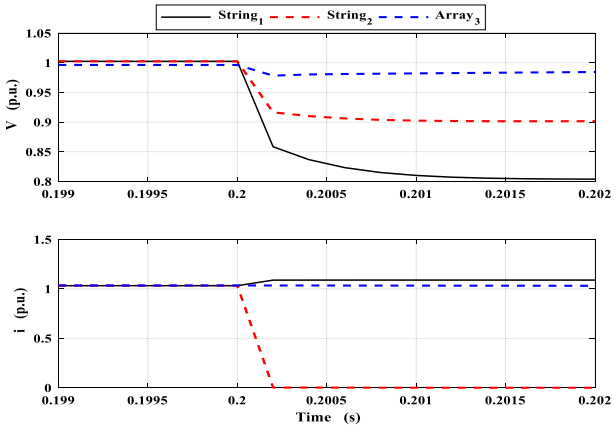

Fig. 7. Voltage and current of the first and second strings and overall array for (High string-to-string) fault with 0 Ω between the first cell of the first string and the third cell of the second string.

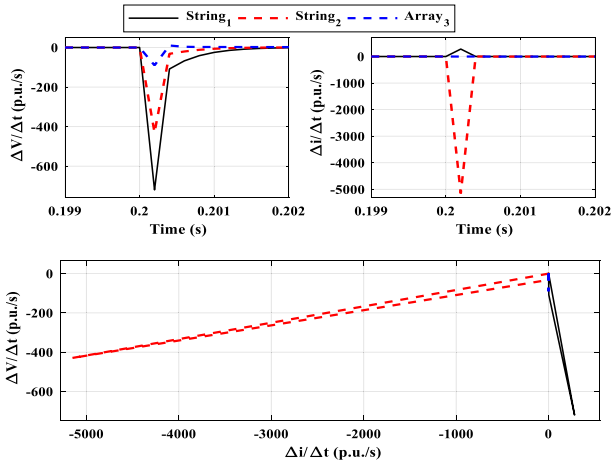

Fig. 8. Rate of change of voltage and current of the first and second strings and overall array for (High string-to-string) fault with 0 Ω between the first cell of the first string and the third cell of the second string.

voltage rate of change of the first and second strings and overall array are −719.7, −429.7 and −90p.u./s, respectively. Accordingly, as shown in Figs. 7 and 8, the current rate of change of the string, which has the lowest number of faulted cells, is positive because the current is increased. This is due to the snubber circuit excited across each diode. Two string diodes are turned off at the end of this state. The current rate of change of the other faulted string is negative as well as the overall array current. The maximum values of the rate of change of current of the first and second strings and overall array are 280.2857, −5155 and −3.9p.u./s, respectively.

Figs. 9 and 10 illustrate the results as the previous state but the fault occurred with 50 Ω resistance (Low string-to-string). In this state, voltages of the faulted strings are changed slightly around 1p.u and are equal to each other. In addition, the healthy strings and array voltages have the same value with the faulted strings. The maximum values of the rate of change of the voltage of the first and second strings and overall array are the same and equal to −21.6 p.u./s. As shown in Figs. 9 and 10, the rate of change of the current is similarly as the previous state with different values. Two string diodes are turned on for this state. However, in this state, the change of the array current is positive contrary to the previous state, which is negative. The maximum values of the rate of change of current of the first and second strings and overall array are 121.7708, −1385.9 and 0.9261p.u./s, respectively.

3.3. Shadow abnormal case

Figs. 11 and 12 present results for a shadow on overall strings (High shadow). From these figures, the voltages of all strings are changed identically from 1p.u. and then exhibit oscillations and then settle down around 0.5p.u. Consequently, currents of all strings are changed from 1p.u. to around 0.9p.u. This state can be defined by the changes of voltages and currents of multiple strings and overall array with high negative values.

On the other hand, in state of low shadow, the shadow can be occurred over one cell to one string. As shown in Figs. 13 and 14, all voltages are changed around 1p.u. Also, all string currents are increased around 1p.u and overall array current is decreased around 1p.u., but the faulted string current is changed from 1p.u. to around 0.5p.u., where this value depends on the shadow value.

3.4. Pole-pole faults

Finally, the fault is assumed to be at positive-to-negative terminals (pole-pole) either solidly or with fault resistance. This fault is occurred at the cathode terminal of the diode to the negative pole. As shown in Figs. 15 and 16, all string voltages go to zero and all currents strings

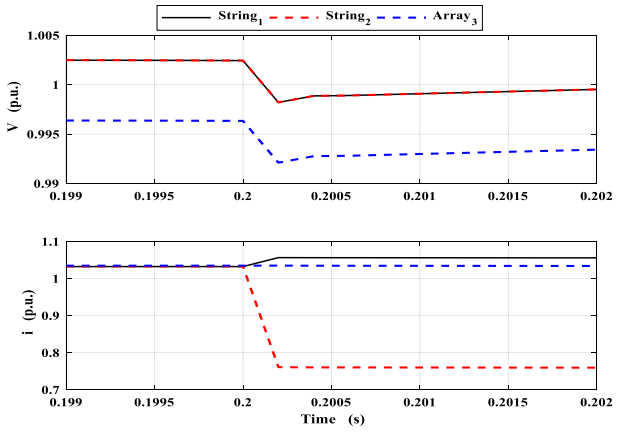

Fig. 9. Voltage and current of the first and second strings and overall array for (Low string-to-string t) fault with 50 Ω between the first cell of the first string and the third cell of the second string.

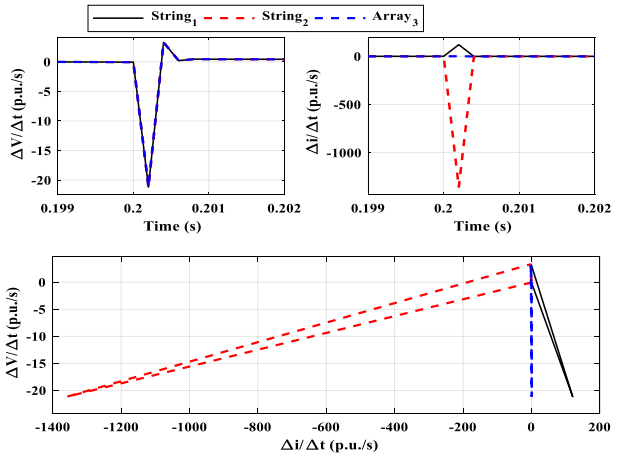

Fig. 10. Rate of change of voltage and current of the first and second strings and overall array for (Low string-to-string) fault with 50 Ω between the first cell of the first string and the third cell of the second string.

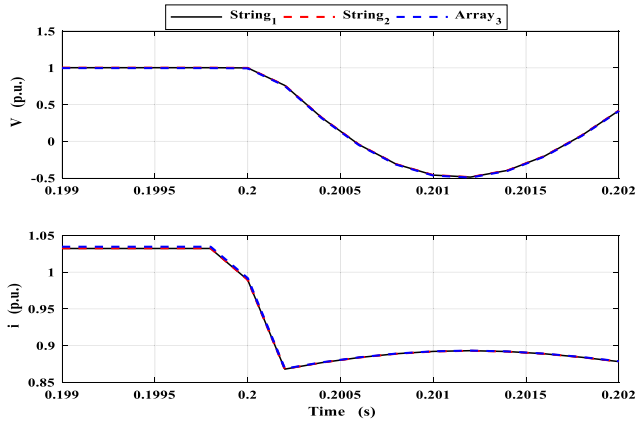

Fig. 11. Voltage and current of the first and second strings and overall array for shadow (irradiation change from 1000 to 800 W/m^2) on the overall array (High shadow).

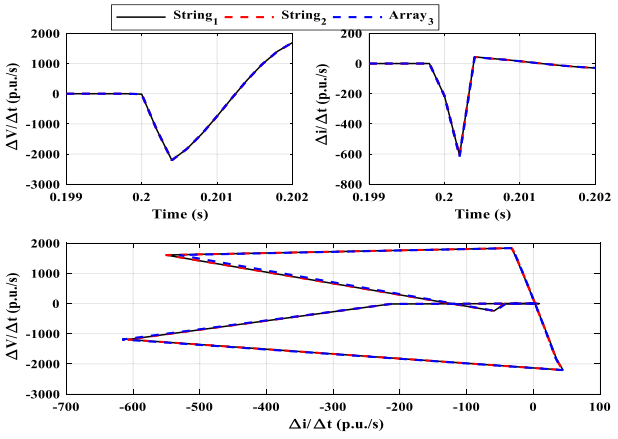

Fig. 12. Rate of change of voltage and current of the first and second strings and overall array for shadow (irradiation change from 1000 to 800 W/m^2) on the overall array (High shadow).

reach the rated short circuit values. At the fault instant, the array current is changed with high value sharply and then goes to zero. This state can be classified as "High current fault". On the other hand, Figs. 17 and 18 present the same fault but all values are occurred with lower levels

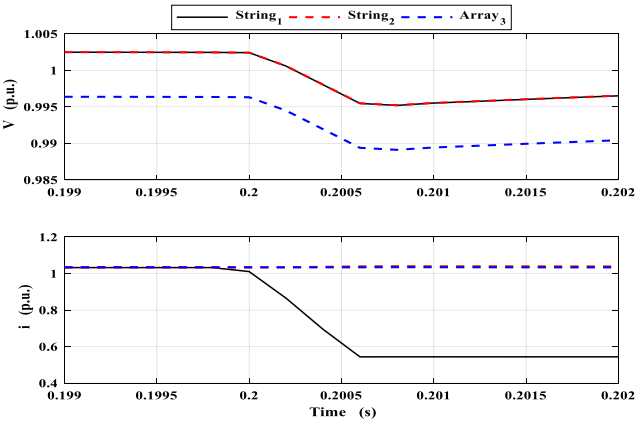

Fig. 13. Voltage and current of the first and second strings and overall array for shadow on one string (Low shadow).

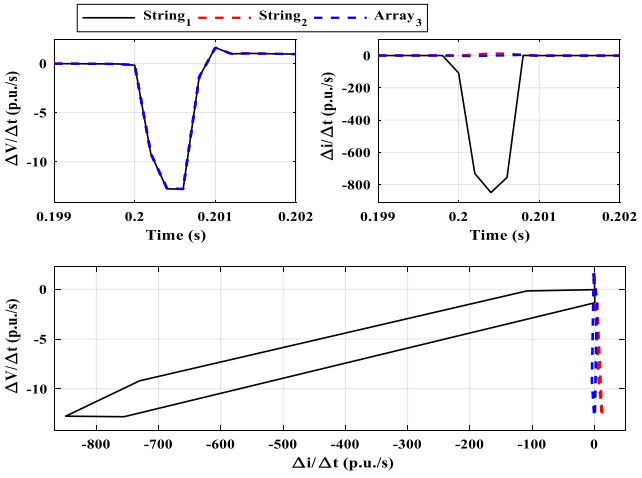

Fig. 14. Rate of change of voltage and current of the first and second strings and overall array for shadow on one string (Low shadow).

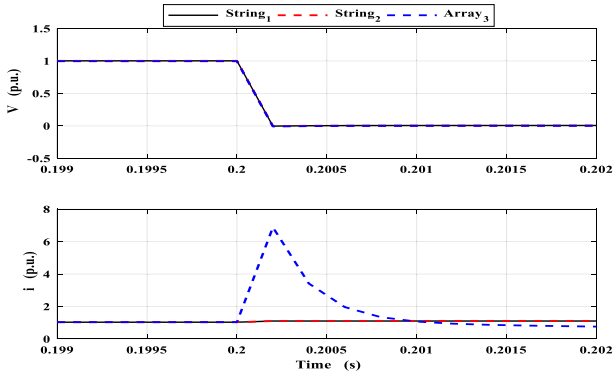

Fig. 15. Voltage and current of the first and second strings and Overall array for (High positive- to-negative terminals) fault with 0 Ω.

because the fault resistance between positive-to-negative terminals equals 50 Ω (Low pole-pole).

3.5. Summery of the different fault cases

Table 2 summarizes the rate of change of voltage and current for strings 1 and 2 and the overall array for different fault cases. Accordingly, each state has special trajectory of changed voltage and current

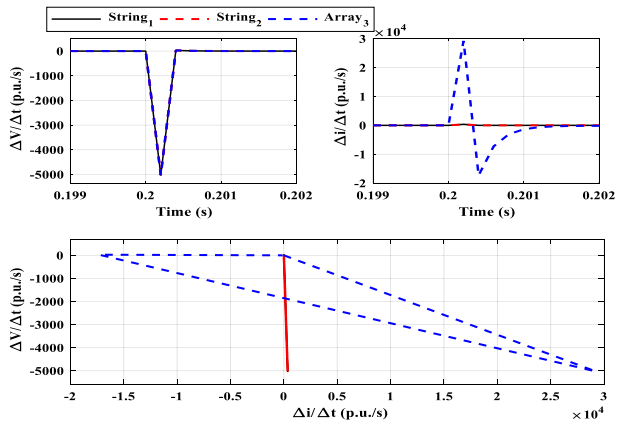

Fig. 16. Rate of change of voltage and current of the first and second strings and overall arrayfor (High positive- to-negative terminals) fault with 0 Ω.

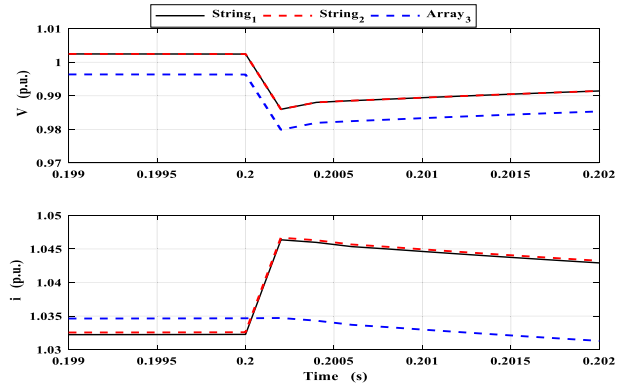

Fig. 17. Voltage and current of the first and second strings and overall array for (Low positive- to-negative terminals) fault with 50 Ω.

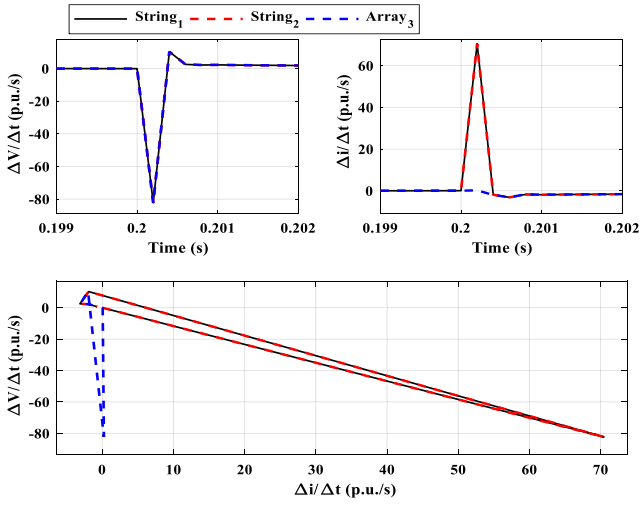

Fig. 18. Rate of change of voltage and current of the first and second strings and overall array for (Low positive- to-negative terminals) fault with 50 Ω.

for each string or for their overall array.

4. The proposed protection technique

As investigated in the previous section, each state of abnormal condition has its own trajectory of voltage and current change. By detecting the values of system states during the transient period after the occurrence of the abnormal state, the type and location of the abnormal state can be determined. Fig. 19 illustrates the flowchart required to classify the abnormal states, which occurred on the PV system according to the proposed measurements. The algorithm starts by the reading of voltages V_j and currents i_j where j is the string index. Also, the overall current of array i_{array} is measured. Therefore, the voltages and currents are measured at sample number k and $k+1$. Then, the rates of change of the measured values over one sample time are calculated. All detected changes in the specified rate of changes should be ranked according to their absolute value. According to the maximum value of change, the discrimination decision is activated.

The first decision is the determination whether the system is in normal state or a certain abnormal state has occurred. This decision is achieved by the continues monitoring of rates of change of voltages and currents to identify whether they exceed a certain threshold value V_{TH1} or not. Here, this value is assumed to equal a certain pick-up value, which initiates the detection algorithm of the abnormal state. If there is not significant change for both currents and voltages, the algorithm indicates "State 0", which means healthy system. If the system is in abnormal case, the states of the system are classified into two main groups "High" and "Low" current of the abnormal case. This classification is achieved by the detection of each string voltage and deciding if it has lower rate of change under certain value V_{TH2}. If the voltage rate of change is less than the predetermined value, then the system is in high current abnormal state, else, the system is in low current abnormal state. In the "High current state", if the changes are in only one string, then the system is in "State 1", i.e., cell-to-cell fault with low resistance. If the rate of change of all currents are more than zero, then the abnormal state is high positive-to-negative terminals fault "State 7". On the other hand, for "High current state", if rate of change of all currents are less than zero, the system is in "State 5", i.e., High shadow. If some rates of change of currents have negative values and some have positive value, the system is in "State 3", i.e., string-to-string fault with low resistance.

The states with "Low current levels" are mainly determined according the rate of change of voltage if it is higher than V_{TH2}. Then, if one rate of change (n) of current is less than zero and some rates (m, g) are positive, while these rates aren't equal (the negative rate and the highest positive rate indicate the faulted strings), then the system is in "State 4", i.e., string to string fault with high resistance. Else, if the overall array rate of change of its current is more than zero, then the system is in "State 8", i.e., low positive-to-negative terminals fault. Else, if the overall array rate of change of its current is less than zero, then the system is in "State 6", i.e., low shadow state. Else, the system is in "State 2", i.e., cell-to-cell fault with high resistance. To differentiate between the internal positive-to-negative faults on a certain array and the external DC bus fault or external three phase fault in AC grid, the techniques applied for each array should be coordinated. The coordination detects whether the rate of change of voltage has big negative value for all arrays simultaneously or not. Therefore, it means that the abnormal state is global for all arrays and, consequently, there is an external fault on the main DC bus or external fault in AC grid.

5. Threshold determination for the proposed technique

According to the proposed technique, three thresholds should be determined. The first and second thresholds are the V_{TH1} and I_{TH}, respectively, which distinguish between the healthy and the abnormal conditions. The proposed technique is sensitive for any abnormal conditions occurred in the adopted array, and it should be stable for the external faults and the normal conditions as well as normal variations. The third threshold V_{TH2} is used to discriminate between low-and high-level states. These cases are summarized in Table 3.

The solidly pole-pole fault at any other array represents an abnormal condition, which is an external fault and the proposed technique should be stable against it. The second column of Table 3 shows the rate of

Table 2
Summary of different fault cases occurred at 0.2 s.

State	1 String1 Cell2-Cell3	2 Cell1-Cell2	3 String1 Cell1- String2 Cell3	4 String1 Cell1- String2 Cell3	6 Shadow String1 Cells1 &2	5 Shadow all Array3	7 Pole-Pole	8 Pole-Pole
R_f	0	50 Ω	0	50 Ω	–	–	0	50
$\Delta V_1/\Delta t$	−4459.4	−7.79	−719.70	−21.6	−12.8	−2218	−502.7	−82.29
$\Delta i_1/\Delta t$	−5273.8	−469.05	280.29	121.77	−849.1	−770.5	362	70.48
$\Delta V_2/\Delta t$	−94.9	−7.77	−429.70	−21.6	−12.77	−2218	−502.7	−82.29
$\Delta i_2/\Delta t$	79.24	7.62	−5155.00	−1385.9	12.6	−608	360	70.48
$\Delta V_t/\Delta t$	−94.9	−7.77	−90.00	−21.6	−12.77	−2218	−502.7	−82.29
$\Delta i_t/\Delta t$	−3.7	0.312	−3.9	0.93	−4.08	−616.1	31,572	0.23
D. T.	0.2 ms	0.1 ms	0.1 ms	0.1 ms	0.4 ms	0.2 ms	0.1 ms	0.1 ms

* D. T. is the detecting time.

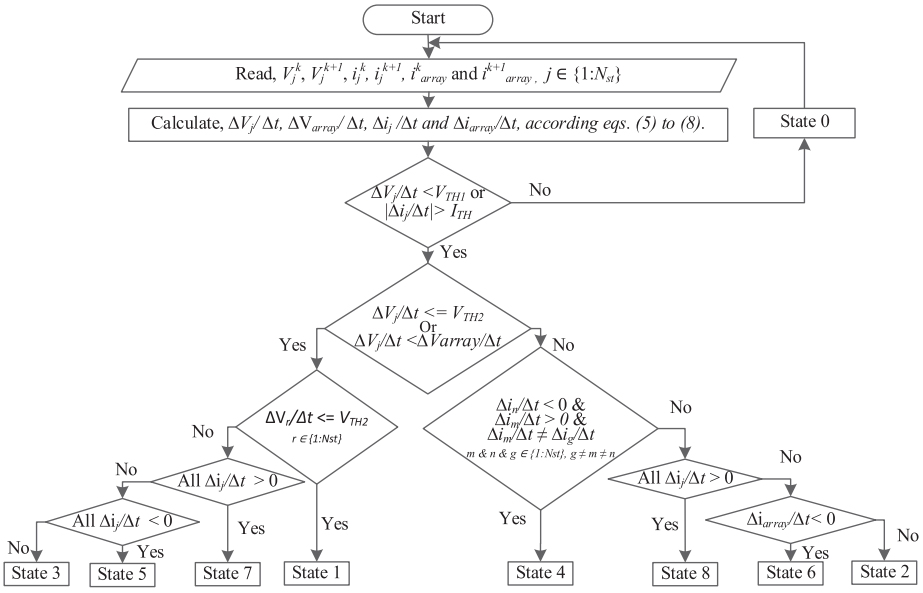

Fig. 19. The flowchart for fault classification of the proposed technique.

Table 3
Threshold values determination for healthy and faulty Conditions and Low and High classification.

Event	Healthy and faulty conditions			Low and High Classification					
	Pole-Pole Array 1	Load increase 0.5p.u	Irrad. 1000–500 W/m^2 Array 3	Cell2-Cell3-String1					
$R_f(\Omega)$	0	-	-	3	2	1.5	1	0.75	0.5
$\Delta V_1/\Delta t$	−0.26	−0.11	−8.3	−71	−84	−91.6	−95.8	−96.9	−157.7
$\Delta i_1/\Delta t$	0.27	0.12	−0.33	−3954.8	−4608	−5040.5	−5160.9	−5160.1	−5162.5
$\Delta V_2/\Delta t$	−0.26	−0.11	−8.3	−71	−84	−91.6	−92.7	−92.8	−92.9
$\Delta i_2/\Delta t$	0.27	0.12	−0.33	58.37	67.03	71.6	72.39	72.54	72.78
$\Delta V_3/\Delta t$	−0.26	−0.11	−8.3	−71	−84	−91.6	−92.7	−92.8	−92.9
$\Delta i_3/\Delta t$	0.27	0.112	−0.33	58.37	67.03	71.6	72.39	72.54	72.78
$\Delta V_t/\Delta t$	−0.26	−0.11	−8.3	−71	−84	−91.6	−92.7	−92.8	−92.9
$\Delta i_t/\Delta t$	0.08	0.11	0.08	1.42	2.58	4.63	−6.9	−6.7	−5.95
V_{TH1}		**−17p.u./s**		V_{TH2}			**−95p.u./s**		
I_{TH}		**17p.u./s**							

change of voltage and current of the first, second and third strings and overall array of adopted array (array3) for positive-to-negative terminal fault at array 1. The rates of change of voltage of all strings and overall array have the same value, which equals −0.26p.u./s while, the rates of change of current of all strings have the same value, which equals 0.27p.u./s.

The normal variations can be represented as sudden change of load and change of the irradiation. The third column of Table 3 and Fig. 20 show the rate of change of voltage and current of strings and overall array for sudden increase of load by 0.5p.u. (200 kW) at the AC grid. The

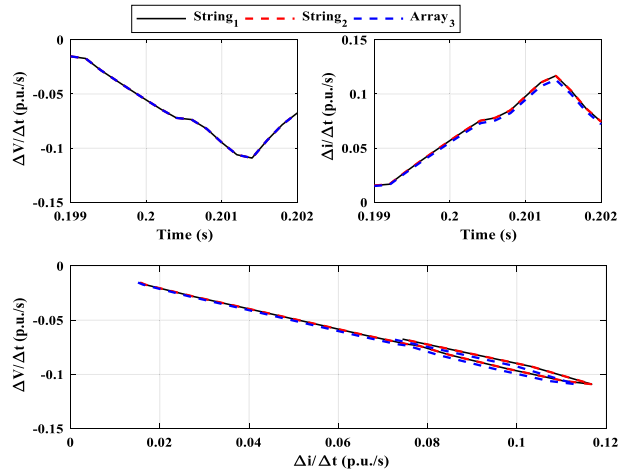

Fig. 20. Rate of change of voltage and current of the first and second strings and overall array for sudden change of load by 0.5p.u.

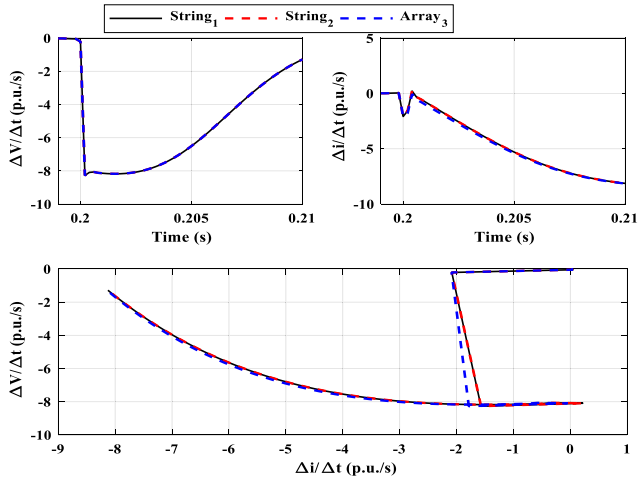

Fig. 21. Rate of change of voltage and current of the first and second strings and overall array for change of irradiation from1000 to 500 W/m$^{2.}$

rate of change of voltages and currents are small due to implementation of MPPT. The fourth column of Table 3 and Fig. 21 show the same results for irradiation change from1000 to 500 W/m^2 (0.5p.u.) at the adopted array. As shown in this figure, the rate of change of voltages are decreased to −8.3p.u./s and rate of change of currents are increased to −0.33p.u./s. Then, rate of change of voltages are increased to −0.33p.u./s, while, the rate of change of currents are decreased to −8.3 p.u./s.

Cell-to-cell fault at single string with variable fault resistance is used to discriminate between low-and high-level states. From the different cases, which are mentioned in Table 2 and the special case in Table 3 that is cell2-cell3 of string1, the voltages rate of change of the faulty string is equal to the healthy and the overall array for high resistance. This is because the diode is in ON state, and vice versa. The rate of change of voltage which makes the diode turns off should be larger than −91.6p.u./s.

The thresholds V_{TH1} and I_{TH} can be set at −17 and 17p.u./s, respectively, which are larger than twice of maximum value either for the external abnormal conditions or for normal variations. This guarantees the stability of the proposed protection technique. The thresholds V_{TH2} is set at −95p.u./s, which is used to discriminate between the low and high states.

6. Validation of the proposed protection technique

The proposed detection technique is tested with the other 14 abnormal cases as shown in Table 4. The validation of the detection technique for various abnormal conditions are carried out by the detection of the voltage and current rate of changes in three strings and in the overall array. By using the proposed technique, each abnormal condition (case) can be detected and classified. The bolded value/s in each case is/are those exceed the threshold value/s. The results of the technique indicate the faulted state by classifying its level as high or low from the rate of change of the voltage. In addition, the rate of change of the current of one string or more as well as of the overall current determine which string is in a certain abnormal state. From this table, each state is defined accurately by the proposed technique. Also, the effect of number of faulted cells with and without fault resistance is presented as shown in cases 1, 2, 6, 7, 8, and 9 for cell-to-cell faults. The technique can detect the state for these cases, while the different number of faulted cells only affects the values level. On the other hand, cases 3, 4 and 11 present string-to-string type with different number of cells in each string. The results of these cases verify that the string with high number of cells has negative value of the rate of change of current. However, the lowest one has negative value of the current rate of change.

Regarding to case 12, from the obtained measurements, it can be noticed that there is one negative rate of change (string 1) and the other rates are positive, while the positive values are not equal. Therefore, the system state is state 4, which has the negative rate of change (string 1) and the string that has the maximum positive rate of change (string 2).

Cases 5 and 13 represent states 8 and 7, which are pole-pole with different fault resistances, high and low, respectively. The proposed technique detects this state accurately, while the resistance value affects the voltages and currents values but with the same trajectory.

For more validation, cases 8 and 9 in Table 4 and Fig. 22 are illustrated by comparing the rate of change of voltage and current trajectory for states 1 and 2. The two cases have the same fault type but with different fault resistance (Cell2-Cell4 of string2). The subplot (1, 2) of Fig. 22 shows that only string 2 is faulted. The voltage and current are changed for state 1 'black color', which is enough to detect this state. On the other hand, the current only is changed for state 2 'red color'. This is required to check the trajectory of array currents, which may be positive or negative. The subplot (2, 2) of Fig. 22 shows that the current change goes to positive value with the red color. The other subfigures are slightly changed without affecting the technique decision.

Furthermore, regarding cases 9 and 10, Table 4 and Fig. 23 show a comparison of rate of change of voltage and current trajectory for states 2 and 6. The two cases have the same fault level (Low). The first case is Cell2-Cell4 of string2 with 50 Ω fault resistance, while the second fault is a shadow on string by changing the irradiation from (1000–800 W/m^2). The subplot (1, 2) of Fig. 23 demonstrates that only string2 is faulted. The current is changed for states 2 and 6, which is not enough to detect these states. For each of them, it is required to check the trajectory of array currents, which may be positive or negative. The subplot (2, 2) of Fig. 23 shows that the current change goes to positive value 'red color' for state 2. However, the current change goes to negative value 'black color' for state 6. Also, other subfigures are slightly changed without affecting the technique decision.

For more validation, according to cases 11 and 13, Table 4 and Fig. 24 illustrate a comparison of rate of change of voltage and current trajectories for states 3 and 7. The two cases have the same level (High) since the voltage rate of change is higher than the predetermined threshold value (V_{TH2} = −95p.u./s). The first case is string1-string2 with 2 Ω fault resistance, while the second fault is pole-pole with 6 Ω fault resistance. The subplots (1, 1) and (1, 2) of Fig. 24 show that only string 2 is faulted 'red color'. This is enough to detect this state, while the trajectory of current goes to positive in sting1 and to negative for string 2. This case represents the state 3. On the other hand, the trajectory of

Table 4
Summary of different abnormal cases.

Case	1	2	3	4	5	6	7	8	9	10	11	12	13	14
Event	String2 Cell0-Cell5	String2 Cell0-Cell5	String1-Cell1 String2-cell3	String1-Cell4 String2-cell3	Pole-Pole	String1 Cell1-Cell2	String2 Cell2-Cell4	String2 Cell2-Cell4	String2 Cell2-Cell4	Shadow String2	String1-Cell1 String2-cell3	String1-Cell4 String2-cell3	Pole-Pole	3-Ø AC
$R_f(\Omega)$	0	60	5	5	60	50	50	2	60	–	2	60	6	0
$\Delta V_1/\Delta t$	−95.7	−68	**−390.3**	**−537.8**	**−67.56**	−7.77	−40	−94.5	−18.5	−12.34	**−580**	−18.5	**−944781**	−757.9
$\Delta i_1/\Delta t$	79.57	60	**269.19**	**−5152.5**	**59.64**	**−469**	37.2	77.42	17.89	12.51	**276.2**	**−1339.8**	**260.21**	16.75
$\Delta V_2/\Delta t$	**−5012.1**	−68.2	**−114.1**	**−89.9**	**−67.56**	−7.77	−40	**−780.6**	−18.5	−12.34	**−304**	−18.5	**−944781**	−757.9
$\Delta i_2/\Delta t$	**−5209.3**	**−3829**	**−5145.7**	**292.43**	**59.64**	7.62	**−2329.6**	**−5154.5**	**−1103.2**	**−825.1**	**−5150.9**	**254.59**	**260.21**	16.75
$\Delta V_3/\Delta t$	−95.7	−68	−90.1	−89.8	**−67.56**	−7.77	−40	−94.5	−18.5	−12.34	−90	−18.5	**−944792**	−757.9
$\Delta i_3/\Delta t$	79.57	60	74.3	74.16	**59.64**	7.62	37.2	77.41	17.89	12.51	74.33	**17.9**	**260.21**	16.75
$\Delta V_t/\Delta t$	−95.7	−68	−90.1	−89.8	**−67.56**	−7.77	−40	−94.5	−18.5	−12.34	−90	−18.5	**−944792**	−757.9
$\Delta i_t/\Delta t$	0.06	**0.91**	0.81	0.7	**0.93**	**0.31**	**1.2**	0.759	**0.85**	**−3.09**	−3.9	0.7557	**29,216**	0.079
State	String2 Cell-Cell High 1	String2 Cell-Cell Low 2	String1 String2 High 3	String1 String2 High 3	Pole-Pole Low 8	String1 Cell-Cell Low 2	String2 Cell-Cell Low 2	String2 Cell-Cell High 1	String2 Cell-Cell Low 2	String2 Shadow Low 6	String1 String2 High 3	String1 String2 Low 4	Pole-Pole High 7	Pole-Pole High 7

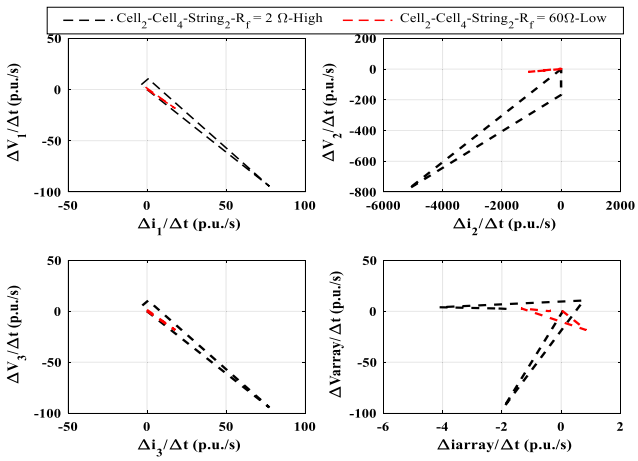

Fig. 22. Comparsion of rate of change of voltage and current trajectory for states 1 and 2.

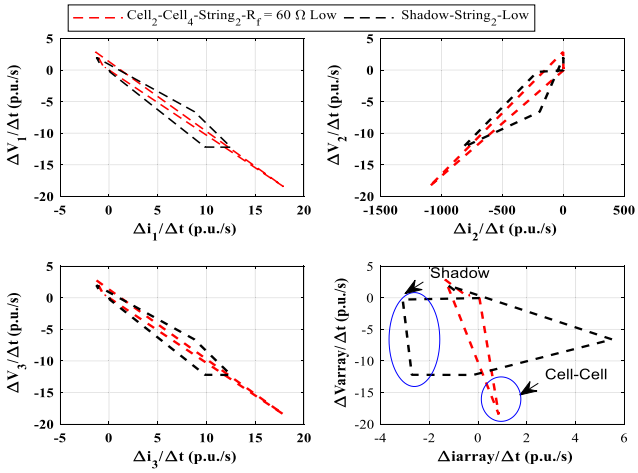

Fig. 23. Comparsion of rate of change of voltage and current trajectory for states 2 and 6.

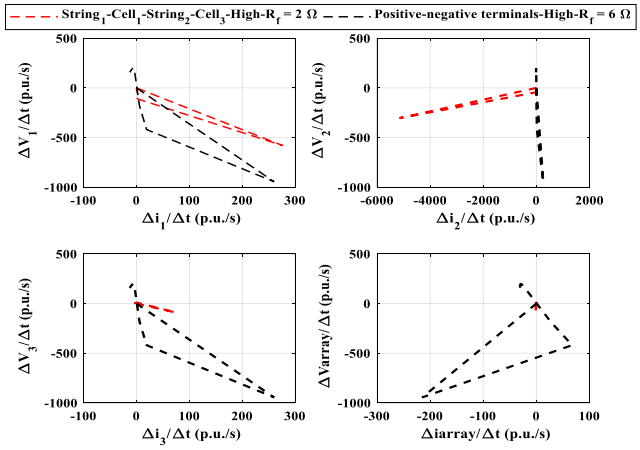

Fig. 24. Comparsion of rate of change of voltage and current trajectory for states 3 and 7.

currents of all strings are changed for state 7 to positive values as well as the overall current trajectory goes to the positive value. This is not enough to detect these states.

Fig. 25 illustrates the rate of change of voltage and current trajectory

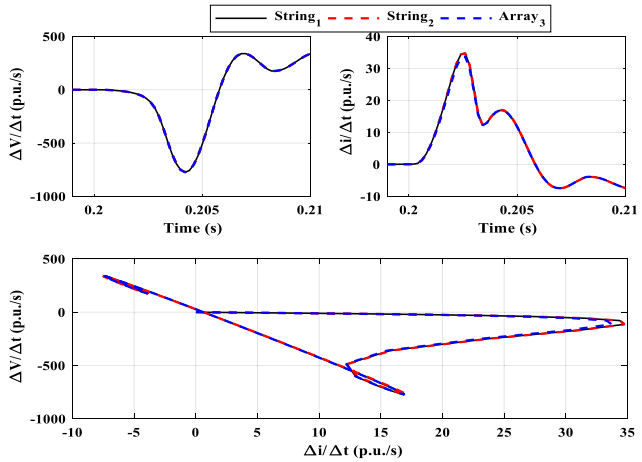

Fig. 25. Rate of change of voltage and current of the first and second strings and overall array for three-phase fault at AC side.

for three-phase fault at AC side. The trajectory of this case has the same locus of the positive–negative terminals fault with or without fault resistance as shown in case 14 in Table 4. As mentioned in Section 4, all arrays send a trip signal with the same fault type. Therefore, the fault is classified as an external fault.

The proposed fault detection and classification technique can be improved to overcome the PV parameters degradation due to aging. The long-time operation affects the parameters of the PV panel with a certain degradation rate [32,33]. In general, the degradation rate determines the deviation of the current panel parameters with respect to the manufacturer's given parameters on the panel [32]. Several uncertainty studies have been conducted to estimate the effect of PV aging on the PV parameters [34]. The mean degradation rates are estimated in these studies to be around 0.17%/year for the open-circuit voltage, 0.78%/year for the short circuit current and 0.56%/year for the fill factor [32]. These rates are considered in this paper to evaluate their effect on the proposed technique sittings. The studied system in Section 2 is tested under parameter degradation due to aging in the operating periods of 10, 15, 20, and 25 years. Table 5 illustrates the variables required to determine the threshold values for different years of operation. It can be noticed that the two thresholds V_{TH1} and I_{TH} are adjusted as double of maximum current and voltage rate of change under sudden normal irradiation change from 1000 to 500 W/m^2. For any studied aging level, these two thresholds are valid to discriminate between healthy and abnormal cases. On the other, the threshold value V_{TH2}, which differentiates between high and low fault cases, should be adjusted due to aging. The differentiation between high- and low-level faults is achieved by applying cell-to-cell fault with a certain high resistance as in Section 5. As shown in Table 5, the value of V_{TH2} should be changed due to the degradation of all variables due to aging. Therefore, V_{TH2} should be slightly changed from −95 to −90, −88.5, −87, and −86p.u./s for aging periods of 10, 15, 20, and 25 years, respectively. In conclusion, the degradation due to aging does not significantly affect the performance of the proposed technique for detection and classification, but the value of only one threshold should be adjusted over the operating lifetime.

7. Experimental results of the proposed technique on a small-scale PV system

For generalization, the proposed fault detection technique is applied on different sizes of PV systems. Here, the PV array system consists of only five parallel strings, which contain two series cells in each string. Table 6 illustrates the data of each panel used in the experimental validation. The simulation results and experimental validation are applied on this system. All extracted results from this system have been scaled to be per unit by dividing string voltages and currents by 260 V and 0.95 A, respectively. According to Table 7 (simulation study), the array is tested under a normal change of irradiation from 1000 to 500 W/m^2.

The first threshold voltage V_{TH1} is set at −8p.u./s to differentiate between healthy and abnormal cases. According to the detected normal irradiation change, the current threshold I_{TH} is set at 8p.u./s. The classification between high and low abnormal cases is achieved by the second threshold voltage V_{TH2}, which is set at −17.7 V.

Fig. 26 shows the voltage and current of the first and second strings and of the overall array when a high cell-to-cell fault with 0 Ω fault resistor is applied between the first and the negative pole of the first string. The rate of change of the voltage and current for this state are shown in Fig. 27. As shown in these figures, the voltage of the faulted string is sharply changed from 1 to around 0.54p.u. On the other hand, the healthy string (string 2) and the voltage across the array (positive to negative terminals), as well as the remaining strings, are slightly decreased. In Fig. 27, the rate of change of the voltage and current can be observed due to the sudden change occurred. It is concluded that the rate of change of voltage and current are very high for the faulted string. However, the healthy strings and overall array are slightly changed

Table 6
PV cell (/Inventux X3-120) data used in experimental validation.

Parameters at standard operation conditions of 1000 W/m^2 irradiation	
Maximum power	120 W
Short circuit current	1.17 A
Open circuit voltage	164 V
Maximum power point current	0.95 A
Maximum power point voltage	126 V

Table 5
Aging effect on threshold values determination for healthy and faulty conditions and Low and High classification.

Event	Irrad. 1000–500 W/m^2 Array 3					Low and High Classification (Cell1-Cell2-String1 fault)				
Aging	0	10	15	20	25	0	10	15	20	25
$\Delta V_1/\Delta t$	−8.3	−7.9	−7.7	−7.6	−7.6	−95.8	−90.5	−88.8	−87.4	−86.1
$\Delta i_1/\Delta t$	−0.33	−0.3	−0.4	−0.4	−0.3	−5160.9	−4757.2	−4549.4	−4354.3	−4152.1
$\Delta V_2/\Delta t$	−8.3	−7.9	−7.7	−7.6	−7.6	−92.7	−88.7	−86.5	−84.5	−82.4
$\Delta i_2/\Delta t$	−0.33	−0.3	−0.4	−0.4	−0.3	72.39	65	60.8	57.4	53.9
$\Delta V_3/\Delta t$	−8.3	−7.9	−7.7	−7.6	−7.6	−92.7	−88.7	−86.5	−84.5	−82.4
$\Delta i_3/\Delta t$	−0.33	−0.3	−0.4	−0.4	−0.3	72.39	64.9	60.7	57.3	53.9
$\Delta V_t/\Delta t$	−8.3	−7.9	−7.7	−7.6	−7.6	−92.7	−88.7	−86.5	−84.5	−82.4
$\Delta i_t/\Delta t$	0.08	0.1	0.1	0.1	0.1	−6.9	−8.2	−9.1	−9.7	−10
V_{TH1}		**−17p.u./s**				V_{TH2}				
I_{TH}		**17p.u./s**				**−95**	**−90**	**−88.5**	**−87**	**−86**

Table 7
Summary of different abnormal cases for a small-scale PV array.

Case	Setting			1	2	3	4	5	6	7
Event	Irrad. 1000–500 W/m^2	String1 Cell1-Cell2		String1 Cell0-Cell1	String1 Cell0-Cell1	String1-Cell1 String2-cell2	String1-Cell1 String2-cell2	Pole-Pole	Shadow string1 Cells 2	Shadow All
$R_f(\Omega)$	-	125	130	0	300	0	300	200	-	-
$\Delta V_1/\Delta t$	0.10	−41.9	−17.7	**−2362.9**	−7.7	**−2525.7**	−7.7	**−44.8**	−3.65	**−30.68**
$\Delta i_1/\Delta t$	−3.53	−2617.7	−2589.9	**−2780.8**	**−1089.2**	**2745.2**	**−2055.7**	**179.3**	**−325.1**	**−365.21**
$\Delta V_2/\Delta t$	0.10	−17.8	−17.7	−20.2	−7.7	**−2518.9**	−7.7	**−44.8**	−3.65	**−30.68**
$\Delta i_2/\Delta t$	−3.53	71.7	71.2	85.3	31.4	**−2896.5**	**997.9**	**179.4**	15.55	**−365.15**
$\Delta V_3/\Delta t$	0.10	−17.8	−17.7	−20.2	−7.7	−4.3	−7.7	**−44.8**	−3.65	**−30.68**
$\Delta i_3/\Delta t$	−3.53	71.6	71.1	82.1	31.4	18.7	31.4	**179.2**	15.55	**−365.23**
$\Delta V_t/\Delta t$	0.10	−17.8	−17.7	−20.2	−7.7	−4.3	−7.7	**−44.8**	−3.65	**−30.67**
$\Delta i_t/\Delta t$	−3.39	−448.3	−443.3	−471	**−185.3**	−18.3	−185.3	−1075.9	**−50.57**	−351.154
State	I_{TH}	**8p.u./s**		String1	String1	String1	String1	Pole-	String2	All
	V_{TH1}	**−8p.u./s**		Cell-Cell	Cell-Cell	String2	String2	Pole	Shadow	Shadow
	V_{TH2}	**−17.7p.u./s**		High 1	Low 2	High 3	Low 4	High 7	Low 6	High 5

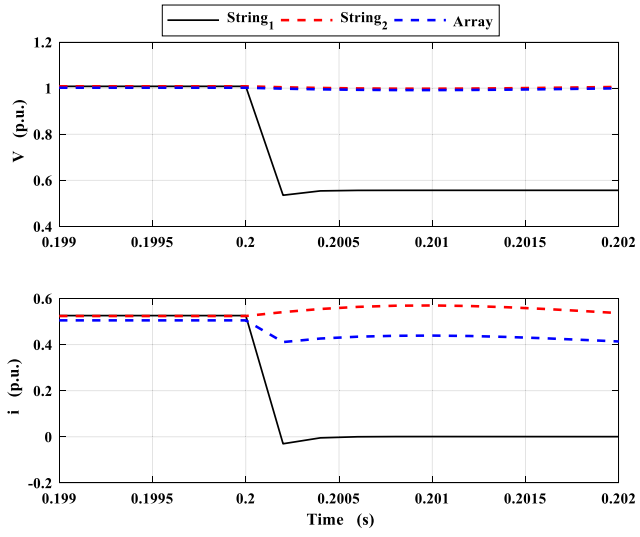

Fig. 26. Voltage and current signals during solidly cell-to-cell fault on string 1 for simulation of a small-scale PV system.

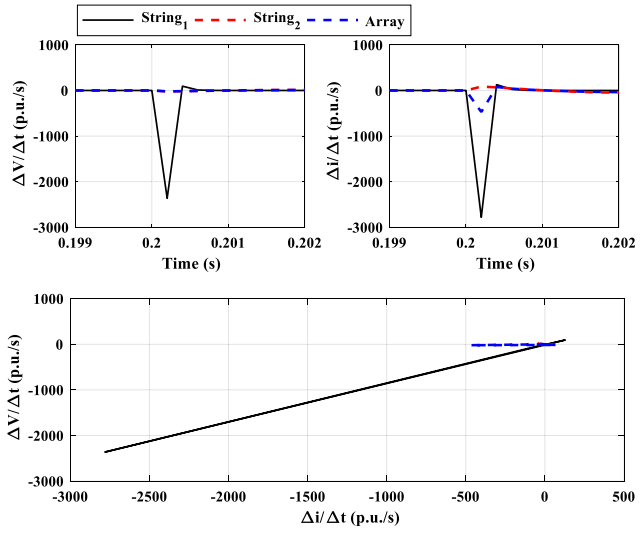

Fig. 27. Rate of change of voltage and current during solidly cell-to-cell fault on string 1 (state 1) for simulation of a small-scale PV system.

around zero. The maximum values of the rate of change of voltage and current for faulty string, healthy string and overall array are shown in Table 7 (case 1). These values occur simultaneously after 0.2 ms from the fault instant. It can be noticed that the rate of change of the array current is high with respect to the previously studied system. In the current PV system, the contribution of one string is relatively high because the power of one string represents 1/5th of the total array power. Table 7 contains the measured variables of the studied system. According to the flowchart in Fig. 19, the proposed technique successfully detects this case as a state 1 (High-cell-to-cell) fault.

Figs. 28 and 29 illustrate the voltage and current and their rate of change of the first and second strings and of the overall array when a low cell-to-cell fault with 300 Ω is applied between the first cell and the negative pole. As shown in these figures, contrary to the previous system, the voltage of the faulted string is changed slightly around 1p.u. Also, in the current system, the healthy string (string 2) and the voltage across the array as well as the remaining strings are slightly decreased. From these figures, all strings voltages and their rate of change are approximately equal to the faulted one. The maximum values of the rate of voltage change of the faulty string, healthy string and overall array are the same and equal to −7.7 p.u./s as shown in Table 7 (case 2) and Fig. 29. Consequently, the faulted string current is sharply changed from 0.525p.u. to around 0.31p.u., while the healthy string and array currents

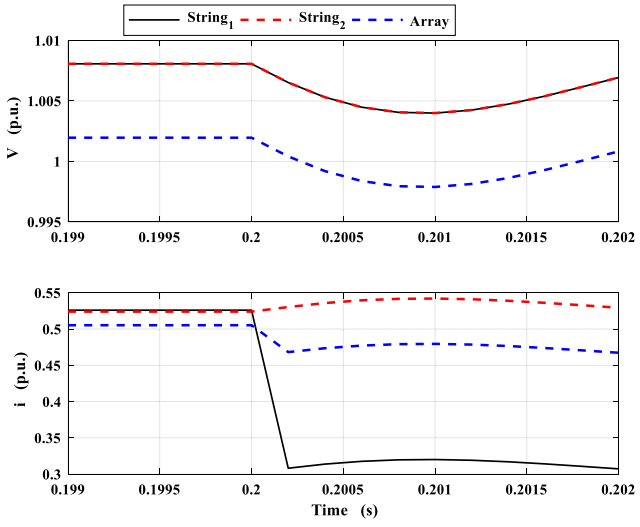

Fig. 28. Voltage and current signals during cell-to-cell fault with 300 Ω resistance on string 1 (state 1) for simulation of a small-scale PV system.

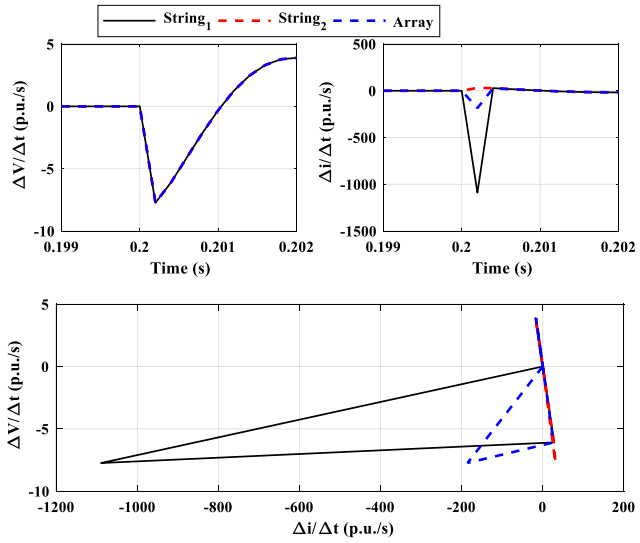

Fig. 29. Rate of change of voltage and current during cell-to-cell fault with 300 Ω resistance on string 1 (state 1) for simulation of a small-scale PV system.

slightly changed around 1 p.u. In this state, the rate of change of the overall array current is negative. The maximum values of the rate of change of current of the faulty string, healthy string and overall array are −1089.2, 31 and −185p.u./s, respectively. It is concluded that the rate of change of current is very high for the faulted string, but the change of voltage is small. However, the healthy strings and overall array are slightly changed around zero.

According to the flowchart to determine the abnormal case, it is difficult to distinguish between low cell to cell state and low shadow state. This difficulty is due to the negative value of rate of change of the total array current (−185.3p.u./s). This phenomenon is due to the low rating of the overall system. Therefore, the contribution of one shaded cell is similar to low cell to cell fault. But the proposed technique is valid for large-scale PV systems.

In the state of low shadow over one cell as shown in Fig. 30, all voltages are changed with the same pattern. The rate of change of current for both total array current and shaded string are negative. The current rate of change of healthy string is positive for a small period. The detected values enable the detection of the system state as low shadow state.

Figs. 31–34 illustrate the rate of change of voltages and currents of

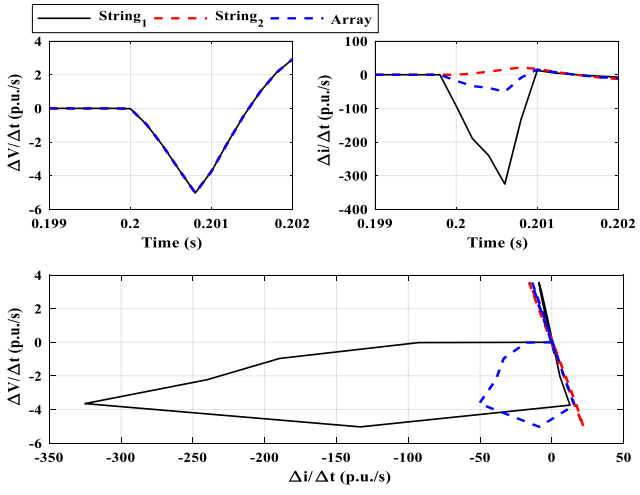

Fig. 30. Rate of change of voltage and current for shadow over one cell (Low shadow) for simulation of a small-scale PV system.

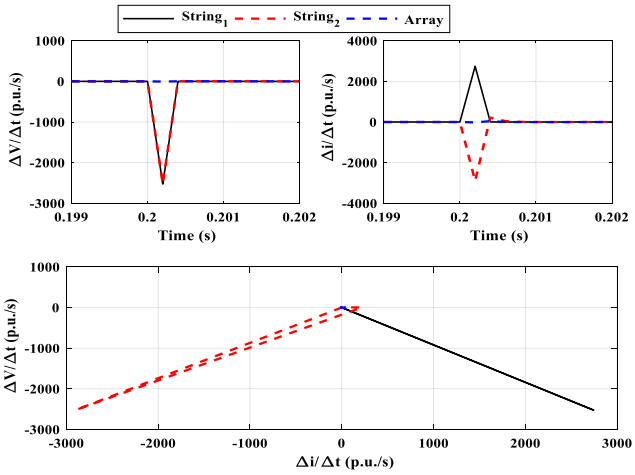

Fig. 31. Rate of change of voltage and current during (High string-to-string) fault with 0 Ω between the cell1-string1 and cell2-stirng2 for simulation of a small-scale PV system.

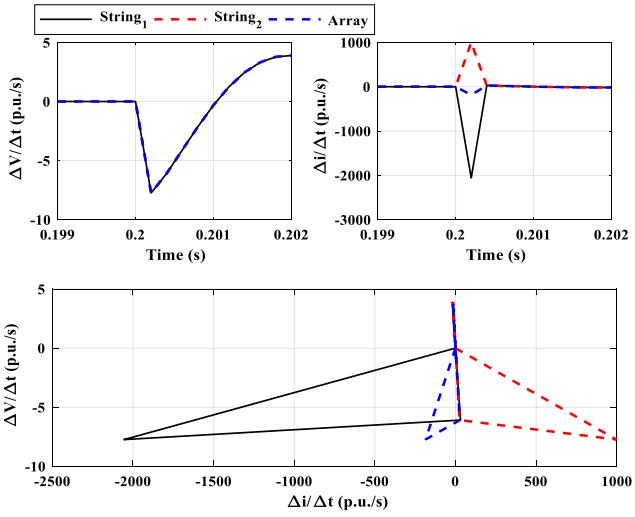

Fig. 32. Rate of change of voltage and current during (Low string-to-string) fault with 300 Ω between the cell1-string1 and cell2-stirng2 for simulation of a small-scale PV system.

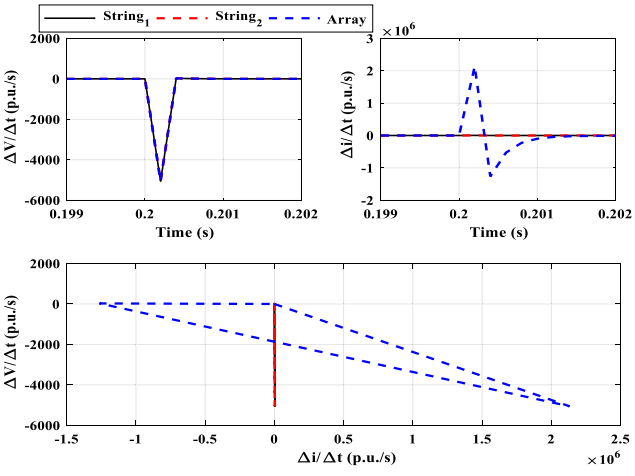

Fig. 33. Rate of change of voltage and current during solidly negative to positive pole (High-Pole-to-pole) for simulation of a small-scale PV system.

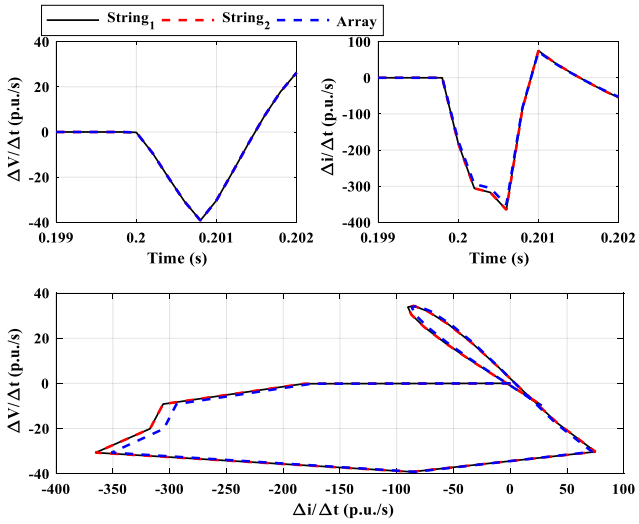

Fig. 34. Rate of change of voltage and current during overall array shadow for simulation of sa mall-scale PV system.

the first and second strings and overall array for high and low string-to-string fault, pole-to-pole fault, and high shadow states, respectively. These cases are summarized also for more clarification in Table 7. If the proposed algorithm, as presented in the flowchart, is applied to these cases, it can efficiently detect the system fault state as 3, 4, 7, and 5 states, respectively.

The proposed technique is applied experimentally to determine the PV system abnormal state. Fig. 35 illustrates the experimental setup of a small PV system installed in the faculty of engineering, Tanta University. As mentioned earlier, the system consists of ten panels forming five parallel strings, where each string contains two series panels. The installed PV system is loaded by a resistive load of 96.6 Ω. The MPPT is not applied in this system.

Five cases have been experimentally conducted to test the proposed fault detection technique. The five cases are high and low cell-to-cell, high and low string-to-string and shadow on one cell. The measured quantities are acquired using the digital oscilloscope and stored in a memory installed in the USB pin/socket. Then, the MATLAB software package is used for plotting these results.

Figs. 36 and 37 illustrate the experimental values of current and voltage and their rate of changes during solidly cell-to-cell fault. By following the flowchart with the measured values, the rate of change of voltage is more than the two threshold voltages. Moreover, voltage rate of change of only one cell is less than the V_{TH2} and, thus, the state is classified as state 1.

Figs. 38 and 39 illustrate the experimental values of the current and voltage and their rate of changes during cell-to-cell fault with a resistive load of 246 Ω. By following the flowchart with the measured values, the rate of change of voltage is less than V_{TH1} but more than V_{TH2}. Thus, the fault is considered as low current abnormal case. Also, there are positive

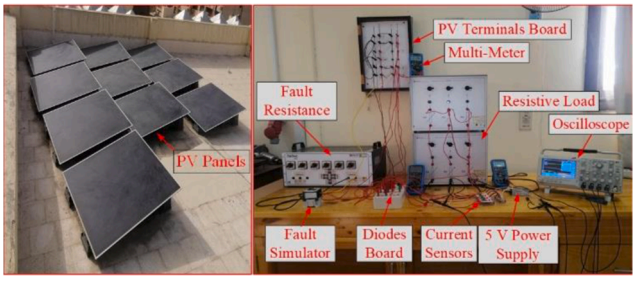

Fig. 35. Experimental setup of a small-scale PV system.

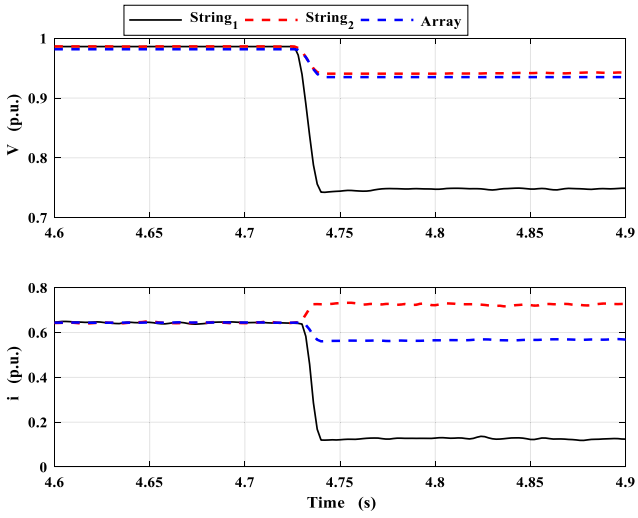

Fig. 36. Experimental values of voltage and current signals during solidly cell-to-cell fault on string 1 (state 1).

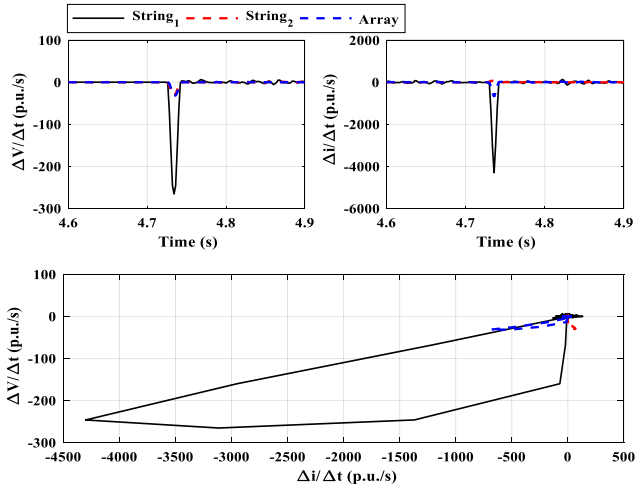

Fig. 37. Rate of change of experimental values of voltage and current signals during solidly cell-to-cell fault on string 1 (state 1).

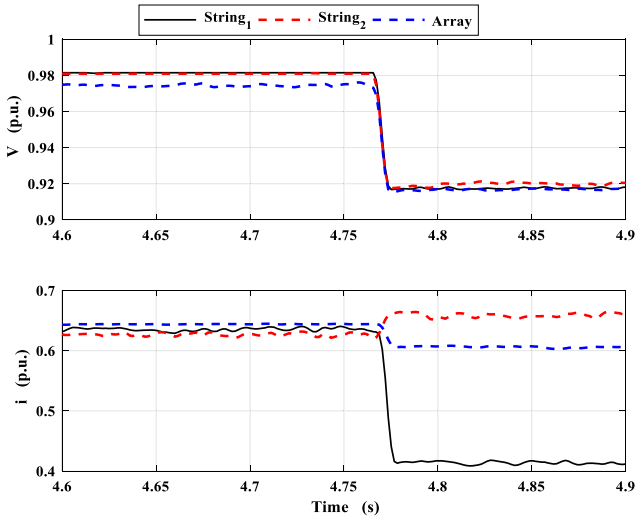

Fig. 38. Experimental values of voltage and current signals during cell-to-cell fault with 246 Ω on string 1 (state 2).

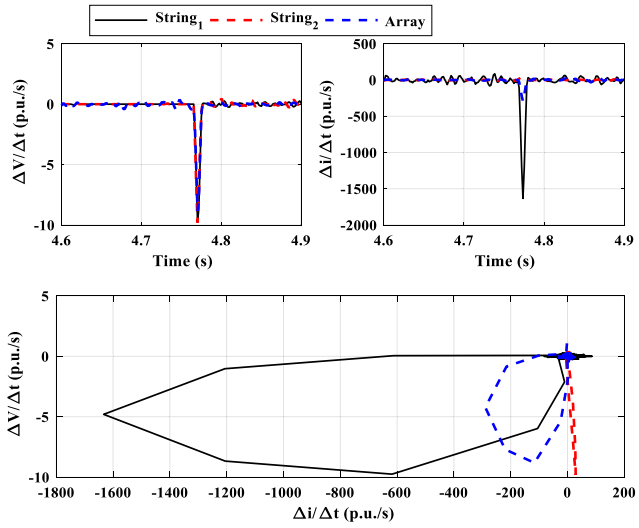

Fig. 39. Rate of change of experimental values of voltage and current signals during cell-to-cell fault with 246 Ω on string 1 (state 2).

and negative rate of change of currents. The positive rates of change of currents are equal. Moreover, each rate of change of strings currents is not positive. In this case, the rate of change of the array current is negative. Therefore, it will be difficult to distinguish between state 2 and state 6. This is because the contribution of one string is relatively high because the power of one string represents 1/5th of the total array power. This result coincides with the previous simulation results. However, with the high rating PV system, it will be easy to distinguish between states 2 and 6.

The proposed technique is stable against noise effect due to the proper setting of the threshold values. The threshold value to detect the system abnormal cases is adjusted to be twice the value of the maximum normal case change. Moreover, it can be noticed that the noise affects the measured values compared with the simulation results. However, this noise does not affect the main trajectory of the current and voltage rate of change. Also, these rates do not exceed the threshold values due to noise. Therefore, the decision of the fault detection and classification is not affected by the noise attack. The deviation between the simulation results and the experimental results is due to the difference between the weather state when the experiment is conducted. The experiment is conducted when the irradiation is about 800 W/m^2. This deviation does not affect the proposed algorithm operation, where it can detect the abnormal states successfully. Moreover, the difference in loading conditions and mode of operation between simulation and experimental presents another challenge. However, the proposed technique has stable performance and correct decisions in most of the conducted cases.

Figs. 40–43 show the experimental values of current and voltage and their rate of changes during the following cases: solidly string-to-string fault and low string-to-string fault with 246 Ω, respectively. According to the obtained results, the proposed technique can successfully detect and classify the system state as 3 and 4, respectively.

Table 8 introduces a comparison between the proposed model and related works in [27], [28] and [29]. The proposed model identifies and classifies different array faults with different low and high states. The advantages of the proposed model can be summarized as follows:

Simplicity: the proposed model requires only three threshold levels to classify different array fault types and shadow faults.
Scalability: the proposed model does not require a training dataset sample. It is built based on different PV system scales.
Sensitivity: the proposed model is capable to detect and classify array and shadow faults with both low- and high-level states.

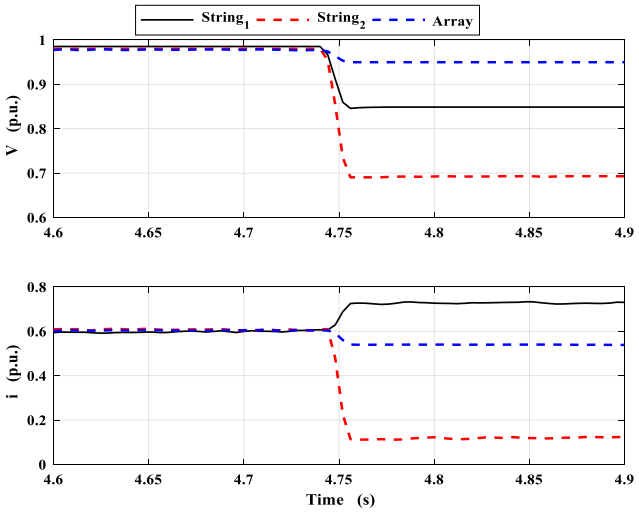

Fig. 40. Experimental values of voltage and current signals during solidly string-to-string fault between the first and second strings (state 3).

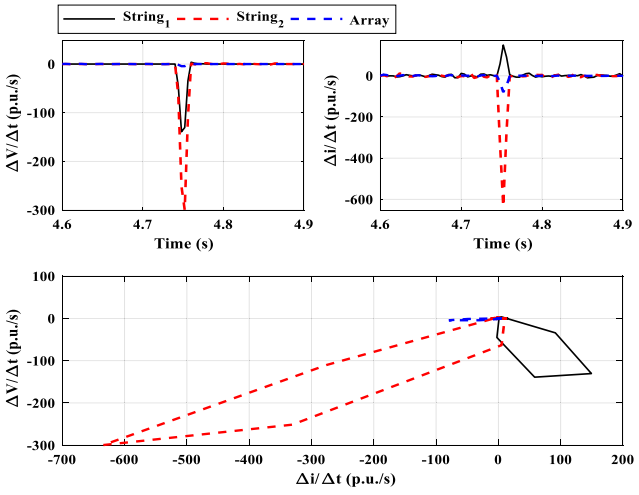

Fig. 41. Rate of change of experimental values of voltage and current during solidly string-to-string fault between the first and second strings (state 3).

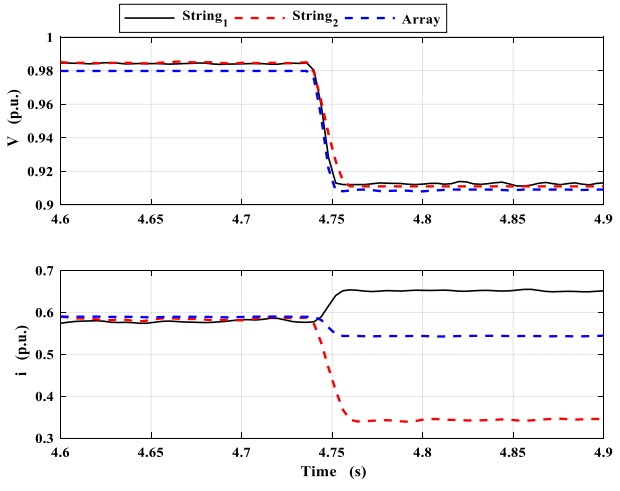

Fig. 42. Experimental values of voltage and current signals during (low string-to-string fault) with 246 Ω between the first and second strings (state 4).

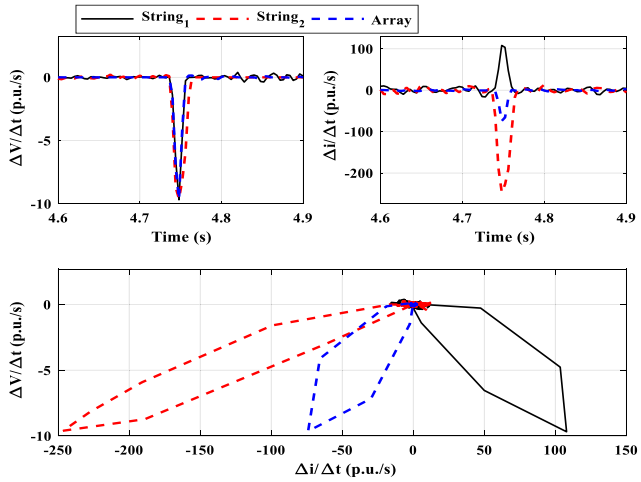

Fig. 43. Rate of change of experimental values of voltage and current during (low string-to-string fault) with 246 Ω between the first and second strings (state 4).

Table 8
Comparisons between proposed model and other techniques.

State	[27]	[28]	[29]	Proposed Model
Is high cell–cell considered?	No	No	Yes	Yes
Is low cell–cell considered?	No	No	Yes	Yes
Is high string-string considered?	Yes	Yes	Yes	Yes
Is low string-string considered?	No	No	Yes	Yes
Is high shadow considered?	Yes	Yes	Yes	Yes
Is low shadow considered?	Yes	Yes	Yes	Yes
Is high pole-pole considered?	No	No	No	Yes
Is low pole-pole considered?	No	No	No	Yes
Is inverter side fault considered?	No	No	No	Yes
Is blocking diode considered?	No	Yes	Yes	Yes
Is aging of PV system is considered?	No	No	No	Yes
Is islanded operation considered?	No	Yes	Yes	Yes
Fault detecting time (1–4, 7–8) in ms	10	27	0.2	0.1
Fault detecting time (5–6) in ms	–	–	–	0.4

Flexibility: the proposed model is built to detect and classify PV system faults for both grid-connected and off-grid configurations. The proposed model takes ages of the PV system in consideration.

8. Conclusions

A developed design of grid-connected PV system has been achieved by adding one diode in each PV string. The proposed design is characterized by simplicity and ability to avoid reverse string currents during fault periods. Although the installation of diodes in the PV system has reduced the current levels during faults, this research has developed a detection technique for various abnormal states. According to the rate of changes of voltages and currents of each string and the main array, the developed algorithm can detect and discriminate various abnormal states at different current levels. The studied system has been tested under various abnormal states to specify the trajectory related to each state. Depending on the specified trajectory, the proposed detection technique has been developed. The proposed technique can detect various string faults such as cell-to-cell faults, positive-to-negative terminal faults and string-to-string faults at different current levels. Also, it can discriminate between the low and high levels of shadow. The proposed technique has been developed to detect the state of the system by only three predetermined threshold values, which is a low number related to the number of states. The settings of the developed technique have been determined for the studied system. Then, detailed validation study has been conducted to check the proposed technique under different operating condition. The proposed technique with the detected settings has provided suitable detection and discrimination results. The proposed technique has high degree of sensitivity for internal faults with proper degree of security against external faults. The degradation rate due to aging has been studied to illustrate its effect on the proposed technique sittings. The aging slightly affects only the second threshold voltage, which differentiates between low and high faults levels. The experimental results have proved the validation of the proposed technique to discriminate the type of the abnormal conducted cases.

CRediT authorship contribution statement

Ibrahim B.M. Taha: Software, Validation, Formal analysis, Writing - original draft, Supervision. **Ahmed E. ELGebaly:** Software, Methodology, Investigation, Formal analysis, Resources, Validation. **Hossam A. Abd el-Ghany:** Conceptualization, Software, Validation, Investigation, Resources, Data curation, Writing - review & editing.

Declaration of Competing Interest

The authors declare that they have no known competing financial interests or personal relationships that could have appeared to influence the work reported in this paper.

Acknowledgement

The authors would like to acknowledge the technical support received from Prof. Dr. Ahmed M. Azmy, Prof. Dr. Nagy I. Elkalashy, Eng. Ismail A. Soliman and Eng. Mahmoud M. Akl.

References

[1] Alraddadi M, Conejo AJ. Operation of an all-solar power system in Saudi Arabia. Int J Electr Power Energy Syst 2021;125:106466. https://doi.org/10.1016/j.ijepes.2020.106466.
[2] International Energy Agency. Report; July 2017.
[3] Patsalides M, Stavrou A, Efthymiou V, Georghiou GE. Towards the establishment of maximum PV generation limits due to power quality constraints. Int J Electr Power Energy Syst 2012;42(1):285–98. https://doi.org/10.1016/j.ijepes.2012.03.043.
[4] Snapshot of Global PV Markets 2020. International Energy Agency (IEA), Report IEA-PVPS T1-37; 2020. https://ieapvps.org/snapshot-reports/snapshot-2020/.
[5] Nancy H. Terawatt-scale photovoltaics: Trajectories and challenges. Science 2017;356:141–3.
[6] Gokmen N, Karatepe E, Celik B, Silvestre S. Real-time fault detection in PV systems under MPPT using PMU and high frequency multi-sensor data through online PCA-KDE-based multivariate KL divergence. Int J Electrical Power Energy Syst 2021;125:106457.
[7] Saha S, Haque ME, Tan CP, Mahmud MA, Arif MT, Lyden S, et al. Diagnosis and mitigation of voltage and current sensors malfunctioning in a grid connected PV system. Int J Electr Power Energy Syst 2020;115:105381. https://doi.org/10.1016/j.ijepes.2019.105381.
[8] Nahas EW, Mansour DA, Abd el-Ghany HA, Eissa MM. Developing A Smart Power-Voltage Relay (SPV-Relay) with no Communication System for DC Microgrids. Electric Power Syst Res 2020;187.
[9] Davarifar M, Rabhi A, El-Hajjaji A. Comprehensive modulation and classification of faults and analysis their effect in DC side of photovoltaic system. Energy Power Eng 2013;5:issue 04.
[10] Hua Y, Gao B, Sonc X, Tian G, Li K, He X. Photovoltaic fault detection using a parameter based model. Sol Energy 2013;96:96–102.
[11] Silvestre S, Silva M, Chouder A, Guasch D, Karatepe E. New procedure for fault detection in grid connected PV systems based on the evaluation of current and voltage indicators. Energy Convers Manage 2014;86:241–9.
[12] Silvestre S, Kichou S, Chouder A, Nofuentes G, Karatepe E. Analysis of current and voltage indicators in grid connected PV (photovoltaic) systems working in faulty and partial shading conditions. Energy 2015;86:42–50.
[13] Hachana O, Tina G, Hemsas K. PV array fault Diagnostic Technique for BIPV systems. Energy Build 2016;126:263–74.
[14] Ventura C, Tina G. Utility scale photovoltaic plant indices and models for on-line monitoring and fault detection purposes. Electr Power Syst Res 2016;136:43–56.
[15] Dhimish M, Holmes V, Mehrdadi B, Dales M. Simultaneous fault detection algorithm for grid-connected photovoltaic plants. IET Renew Power Gener 2017;11:1565–75.
[16] Jain P, Poon J, Singh J, Spanos C, Sanders S, Panda S. A Digital Twin Approach for Fault Diagnosis in Distributed Photovoltaic Systems. IEEE Trans Power Electron 2020;35:940–56.

[17] Bonsignore L, Davarifar M, Rabhi A, Tina G. Neuro-Fuzzy fault detection method for photovoltaic systems. Energy Procedia 2014;62:431–41.
[18] Basnet B, Chun H, Bang J. An Intelligent Fault Detection Model for Fault Detection in Photovoltaic Systems. J Sens 2020:1–11.
[19] Gao W, Wai R. A Novel Fault Identification Method for Photovoltaic Array via Convolutional Neural Network and Residual Gated Recurrent Unit. IEEE Access 2020;8:159493–510.
[20] Taha I, Elkalashy N, Alsharef M, Sabiha N, Metwaly M, Elattar E. Investigation of diode dynamic effect on fault detection of photovoltaic Systems. Sustain Energy Grids Netw. 2020;23:1–10.
[21] Chen Z, Wu L, Cheng S, Lin P, Wu Y, Lin W. Intelligent fault diagnosis of photovoltaic arrays based on optimized kernel extreme learning machine and I-V characteristics. Appl Energy 2017;204:912–31.
[22] Ahmadipour M, Hizam H, Othman M, Radzi M, Chireh N. A Fast Fault Identification in a Grid-Connected Photovoltaic System Using Wavelet Multi-Resolution Singular Spectrum Entropy and Support Vector Machine. Energies 2019;12:1–18.
[23] Fazaia R, Abodayehb K, Mansouria M, Trabelsic M, Nounoua H, Nounoud M, et al. Machine learning-based statistical testing hypothesis for fault detection in photovoltaic systems. Sol Energy 2019;190:405–13.
[24] Dhibi K, Fezai R, Mansouri M, Trabelsi M, Kouadri A, Bouzara K, Nounou H, Nounou M. Reduced Kernel Random Forest Technique for Fault Detection and Classification in Grid-Tied PV Systems. IEEE J Photovol 2020;10:1864–71.
[25] Gao W, Wai R, Chen S. Novel PV Fault Diagnoses via SAE and Improved Multi-Grained Cascade Forest with String Voltage and Currents Measures. IEEE Access 2020;8:133144–60.
[26] Huang J, Wai R, Yang G. Design of Hybrid Artificial Bee Colony Algorithm and Semi-Supervised Extreme Learning Machine for PV Fault Diagnoses by Considering Dust Impact. IEEE Trans Power Electron 2020;35:7086–99.
[27] Saleh KA, Hooshyar A, El-Saadany EF, Zeineldin HH. Voltage-based protection scheme for faults within utility-scale photovoltaic arrays. IEEE Trans Smart Grid 2017;9(5):4367–82.
[28] Khoshnami A, Sadeghkhani I. Two-stage power-based fault detection scheme for photovoltaic systems. Sol Energy 2018;176:10–21.
[29] Li C, Yang Y, Zhang K, Zhu C, Wei H. A fast MPPT-based anomaly detection and accurate fault diagnosis technique for PV arrays. Energy Convers Manage 2021; 234:113950.
[30] https://ch.mathworks.com/help/physmod/sps/examples/400-kw-grid-connected-pv-farm-average-model.html.
[31] MATLAB/toolbox software; 2019.
[32] Bandou F, Arab AH, Belkaid MS, Logerais PO, Riou O, Charki A. Evaluation performance of photovoltaic modules after a long time operation in Saharan environment. Int J Hydrogen Energy 2015;40(39):13839–48. https://doi.org/10.1016/j.ijhydene.2015.04.091.
[33] Dechthummarong C, Wiengmoon B, Chenvidhya D, Jivacate C, Kirtikara K. Physical deterioration of encapsulation and electrical insulation properties of PV modules after long-term operation in Thailand. Sol Energy Mater Sol Cells 2010;94 (9):1437–40.
[34] Golive YR, Zachariah S, Bhaduri S, Dubey R, et al. Analysis and Failure Modes of Highly Degraded PV Modules Inspected during the 2018 All India Survey of PV Module Reliability. In 2020 4th IEEE Electron Devices Technology & Manufacturing Conference (EDTM), Penang, Malaysia; 2020, p. 1–4. http://dx.doi.10.1109/EDTM47692.2020.9117930.